Arctic summer cloud optical properties and annual sea-ice retreat‡

Authors: Michael Behrenfeld[1*†], Yongxiang Hu[2*†], Ilan Koren[3], Xubin Zeng[4], Kelsey Bisson[1,5], Michael A. Brunke[4], Xiaomei Lu[2], Carl Weimer[6], Meibing Jin[7], Travis Knepp[2], Yuping Huang[8]

Affiliations:

[1] Department of Botany and Plant Pathology, 2071 SW Campus Way, Oregon State University, Corvallis, OR, USA
[2] NASA Langley Research Center, MS 475, Hampton, VA 23681, USA
[3] Department of Earth and Planetary Sciences, Weizmann Institute of Science, Rehovot, Israel
[4] Department of Hydrology and Atmospheric Sciences, University of Arizona, Tucson, AZ, USA
[5] Ocean Biology and Biogeochemistry Program, NASA Headquarters, Science Mission Directorate, Earth Science Division, Mail Suite 3Y35, 300 E St., SW, Washington, D.C. 20546-0001.
[6] BAE Systems, Inc., 1600 Commerce Street, Boulder, CO, USA
[7] The International Arctic Research Center, University of Alaska, Fairbanks, AK, USA
[8] Quantum Computing Incorporated, 5 Marine View Plaza, Suite 214, Hoboken, NJ 07030

*Corresponding authors

† These authors contributed equally to this work.

Changes in Arctic sea-ice areal coverage have major ecological, climate, and economic implications and are driven by diverse natural and anthropogenic forcings acting over a wide range of time scales. Cloud-related variability in atmospheric radiative budgets is suspected to be particularly important in year-to-year changes in ice melt. Here, we describe a decade of pan-Arctic satellite light detection and ranging observations indicating that shortwave transmittance differences of low-altitude clouds play a key role in ice retreat through summer. These summer cloud transmittance differences result in surface solar radiation budget changes comparable to melt energy requirements for observed year-to-year changes in September sea-ice extent. As a working hypothesis, we propose that variations in summer cloud optical properties reflect a combination of positive- and negative-feedback processes involving aerosol cloud condensation nuclei. Our findings suggest a delicate atmosphere-biosphere-cryosphere balance where minor perturbations in Arctic cloud properties can have major implications on September sea-ice extent.

Main text:

Arctic sea-ice cold-season formation and warm-season retreat are governed by diverse oceanic and atmospheric processes[1-5] and exhibit multi-year to multi-decadal teleconnections with lower latitude climate oscillations [e.g., Atlantic multidecadal oscillation, North Atlantic Oscillation, Pacific decadal oscillation, El Niño–Southern Oscillation][5-8]. Beyond these natural cycles, anthropogenically-forced global warming has added a sustained trend of declining Arctic sea-ice that is clearly imprinted in the satellite record[9-10]. Superimposed on all these longer-term oscillations and trends are strong interannual variations in sea-ice extent. These year-to-year changes present very real constraints on the productivity[11-12] and survival of Arctic organisms ranging from microscopic plankton to 'charismatic megafauna' (e.g., polar bears, whales, seals)[13-15], as well as having implications for ocean circulation[16] and navigation[17]. Variations in atmospheric radiative forcing associated with changing cloud properties are thought to play a vital role in the seasonal retreat of sea-ice to its annual minimum in September[18-21]. Here we describe unique observations from satellite-based light detection and ranging (lidar) measurements that shed new light on Arctic sea-ice dynamics and suggest an important role for summer aerosol-related cloud optical properties in annual ice melt.

Satellite lidar advantage

While observations from passive (i.e., reflected sunlight and emitted longwave radiation) satellite sensors have been instrumental in monitoring interannual changes in sea-ice extent and ocean and atmospheric properties, accurate retrieval of Arctic cloud properties from these measurements is challenging because little contrast may exist between surface and cloud reflectances and thermal contrasts are compromised by frequent temperature inversions[18-19,22]. To overcome these challenges, we examined Arctic cloud properties using measurements from the space-based Cloud-Aerosol Lidar with Orthogonal Polarization (CALIOP) sensor[23] for the period 2008 to 2017 when CALIOP data are most accurate (**Methods**). While its spatial coverage does not match that of passive sensors with large swaths (**Methods**), CALIOP measurements can be particularly valuable for polar research because the technique measures a vertically-resolved return signal from an active laser pulse that clearly distinguishes cloud signals from surface reflections (i.e., rather than relying on surface and cloud reflectance contrasts)[18,24]. CALIOP's cross-polarized and co-polarized signals at 532 nm also provide a direct and accurate measurement of cloud depolarization, enabling assessment of cloud optical depth, reflectance, and transmittance (**Methods**)[25-28]. Due to its large receiver footprint diameter (~90 m at the ground[23]), CALIOP measurements penetrate through most clouds and enable highly accurate retrievals of low-altitude Arctic cloud extinction coefficients through the measured exponential decay rate of its backscattering profiles (**Methods**)[29]. In addition, CALIOP allows discrimination of ice and water scenes and measures subsurface plankton populations[30-31], thus many key atmosphere-biosphere-cryosphere attributes of the Arctic system are captured by a single instrument.

Summer cloud optical properties and ice melt

Previous modeling has suggested that variations in downwelling shortwave (SW) radiation transmittance through low altitude Arctic clouds has the potential to influence summer sea-ice melt[32]. Field observations have shown that changes in optical properties of these clouds can account for multi-day melting events in Greenland[33]. Leveraging the spatial coverage and advanced retrievals of CALIOP, our investigation focuses on pan-Arctic observations of low-altitude (< 3 km) cloud optical properties during the core melt season of June through August (JJA) and their link to interannual variations in September sea-ice extent (SSIE) (i.e., the month of minimum sea ice). During this core melt season, Arctic surface temperatures are near or above 0°C and cloud fraction (CF; the percentage of the sky covered by clouds) is at its annual maximum (> 70%)[18,22,34-35]. Low-altitude clouds predominate during summer[19,22,34], are typically single or double layered[34], and have cloud top temperatures of -20° to 0°C [35-36]. These clouds are most commonly liquid phase clouds but also include mixed phase clouds dominated by liquid water but containing ice particles[36,38-40]. Liquid water content (LWC) of these low altitude clouds tends to be well above the threshold where clouds become opaque to longwave (LW) radiation (i.e., they behave as 'blackbody' LW radiators)[36,41-42], but they do transmit downwelling SW radiation in a manner dependent predominantly on liquid droplet number and droplet size (as opposed to properties of coexisting ice particles)[36-37] (**Methods**).

For the 2008 to 2017 CALIOP record, SSIE was maximal in 2009 (5.1×10^6 km^2) (Fig. 1), minimal in 2012 (3.4×10^6 km^2) (Fig. 1), and fluctuated between these extremes during the other years (Fig. 2a,b, red lines). What we find is that these interannual variations in SSIE are remarkably well correlated with JJA mean low-altitude cloud depolarization ratios [proportional to cloud optical depth (**Methods**)] (Fig. 2a, blue line; $r = 0.85$, $p = 0.002$) and extinction coefficients (Fig. 2b, blue line; $r = 0.88$, $p < 0.001$). The former relationship implies that ice melt is more extensive when summer clouds are more transparent, while the latter relationship suggests that year-to-year changes in cloud optical properties primarily reflect microphysical changes rather than factors such as cloud thickness. Notably, our observed (time-delayed) correlations are considerably stronger than previously reported correlations with spring Arctic CF that accounted for ~25% of SSIE variability[19,43] and we find little to no significant correlations between SSIE and climate oscillations (Table 1 in Methods) or cloud properties observed with passive sensors (Table 2 in Methods) for the 2008 to 2017 period.

Small changes, big effects

While well correlated with SSIE, our observed pan-Arctic mean cloud depolarization and extinction values span a notably constrained absolute range (see y-axes in Fig. 2a,b). Can small variations in summer cloud properties contribute significantly to year-to-year differences in SSIE? To answer this question, we estimated changes in total summertime radiative flux through Arctic clouds using CALIOP optical depth (Extended Data Fig. 1; estimated from depolarization data in Fig. 2a), CF (Extended Data Fig. 2), and surface reflectivity data (**Methods**). This estimate yielded a radiative flux difference between the 2009 maximum sea-ice year and 2012 minimum sea-ice year of 8.42×10^{20} J, which compares closely to the estimated 6.59×10^{20} J change in melt energy necessary to account for the observed 1.7 million square kilometer difference in SSIE between these two years (Fig. 1) (**Methods**). Likewise, we find a strong correlation ($r = 0.96$, $p < 0.001$) between anomalies in summertime radiative fluxes and melt energy requirements for observed SSIE variations across the CALIOP record (Fig. 2c). Thus, small changes in cloud optical properties can indeed play a potentially major role in ice melt. The reason for this is that clouds are pervasive during summer [mean summer CF was 75% for 2008-2017 (Extended Data Fig. 2)], so a change in cloud optical properties impacts surface radiative budgets over a vast expanse of the Arctic region.

Cloud droplets, aerosols, and precipitation

To further understand variations in low-altitude cloud optical properties, we investigated annual cycles in cloud droplet number density (Nd) quantified from CALIOP measured cloud extinction coefficients (**Methods**, Extended Data Fig. 3c). Cloud droplets form when water condenses around aerosol 'nuclei' [44-45] (note, some aerosols also nucleate ice formation in mixed phase clouds[46-47]). As summer Arctic clouds are generally among the cleanest in the world[48] and aerosol-limited[49-50], we were interested in whether low, moderate, and high SSIE years might be distinguished by their annual Nd cycles, thus pointing to an aerosol-basis for year-to-year changes in cloud optical properties. Specifically, the expectation is that cloud droplets will be small and numerous [i.e., elevated depolarization ratio (Fig. 2a)] when Arctic aerosols are relatively abundant, causing clouds to reflect a larger fraction of downwelling shortwave (SW) sunlight [i.e., strong albedo, elevated extinction coefficient (Fig. 2b)], while transmitting little[48,51-52]. Conversely, cloud droplets will be larger but fewer when Arctic aerosols are relatively scarce [i.e., low depolarization ratio (Fig. 2a)], causing SW albedo to be weaker [i.e., low extinction coefficient (Fig. 2b)] and transmittance to be greater[48,51]. In other words, decreased (increased) summer aerosols would increase low-altitude cloud SW transmittance (reflectance), consequently warming (cooling) the surface and accelerating (slowing) ice melt.

CALIOP reveals a pan-Arctic mean Nd cycle exhibiting a rapid late-winter to late-spring increase that is essentially indistinguishable between contrasting SSIE years (Fig. 3a). The annual cycles in Nd for low, moderate, and high SSIE years instead become distinguished during summer. Specifically, the late May through July decrease in Nd (Fig. 3a) is only ~48% for years with high SSIE (Fig. 3a, red line) and 64% for the 2012 SSIE minimum (Fig. 3a, blue line), with Nd declines falling between these values for moderate SSIE years (Fig. 3a, green line). These distinctions in Nd cycles are fully developed by the end of July and then persist through August and September (Fig. 3a). We further find that summer Nd reduction rates for the low, moderate, and high sea ice retreat years are highly and negatively correlated with summer drizzle/rain probabilities ($r = 0.98$, $p = 0.1$) (**Methods**) and that year-to-year variations in summer drizzle/rain probability inversely correlate ($r = -0.71$, $p = 0.02$) with September Nd (Fig. 3c). The relevance of these findings is that precipitation is the primary mechanism removing aerosol cloud condensation nuclei (CCN) from the Arctic atmosphere[52].

A working hypothesis

Figure 2 reveals unprecedentedly high observation-based and time-delayed correlations between Arctic cloud properties and sea ice retreat. In this section, we propose a 'working hypothesis' further interpreting our findings and couched within understanding of specific Arctic annual cycle properties and processes. While this hypothesis remains unproven and does not explicitly encompass all factors influencing Arctic energy budgets (e.g., the complex role of ice particles in cloud properties), our hope is that it motivates future mechanistic modeling and field studies that build upon (or replace) this framework.

Prior to our study, an extensive literature documented key Arctic cloud and ice properties and processes. Briefly, Arctic clouds in winter are optically thin[48], ice clouds are prevalent[22], CF is at its annual minimum[22], and long-range transport is the dominant source of aerosols[52]. These aerosols accumulate into an early-spring 'Arctic haze' because ice-phase precipitation is very inefficient at removing them[52-54]. As sunlight increases during spring, temperatures increase and local marine and terrestrial aerosol sources increase[21,52]. During late spring (April-May), low-altitude cloud coverage increases dramatically[19,22]. Year-to-year changes in late spring CF set a trajectory for sea-ice retreat due to a positive feedback with surface albedo[19-20,42-43]. Specifically, when spring CF is elevated (Fig. 4a), a greater amount of LW radiation is retained near the surface that causes earlier and more rapid ice melting, whereas ice melt is slower and delayed in years with lower spring CF (Fig. 4d) [42,55-57]. The early melting in high CF years is expressed by enhanced liquid water in surface sea-ice[57], increased abundance of melt ponds on ice[43,57-58], and greater open water along sea-ice leads[43]. These changes support further increases in CF[56,59] and drive a decrease in surface albedo[19] that progressively increases the role of SW radiation in ice melting during years with high spring CF (Fig. 4a) compared to years with low spring CF (Fig. 4d)[42-43,56-57]. Our CALIOP record indicates that April-May cloud droplet number density (Fig. 3a) and optical properties (black line/symbols in Fig 2a,b) are relatively invariant between years, implying that variations in springtime aerosol supply are predominantly expressed through changes in CF and consistent with observations from earlier studies that early season surface radiative budgets and ice melt correlate with CF variability (Fig. 4a,d) [19,43].

While the processes described above are relatively well established, year-to-year variations in spring CF generally explain less than 25% of observed variability in SSIE. Here, we speculate on how early spring ice melt may be mechanistically linked to aerosol removal during summer, thus leading to our far greater explained variance (92%, Fig. 2c) in SSIE. We speculate that elevated water vapor following a spring of high CF and enhanced ice melt should (all else being equal) lead to larger average droplet sizes. With a greater propensity to precipitate[60], these larger droplets should more rapidly remove CCN from the atmosphere[53], subsequently favoring even greater average droplet sizes (Fig. 4b). Such a cycle would progressively increase SW transmittance through the low-altitude clouds, thereby augmenting ice melt and leading to significantly greater open ocean area later in the summer. Thus, the springtime 'ice melt-CF' positive feedback described above (Fig. 4a) may be envisioned as a precursor to a second early-summer 'ice melt-cloud optics' positive feedback (Fig. 4b). Summer cloud optical properties will, of course, also be sensitive to changes in aerosol sourcing, and indeed we do observe a correlation between year-to-year changes in Arctic summer aerosol optical depth and Nd (Extended Data Fig. 4). Thus, years with low springtime ice melt (Fig. 4d) and/or high summer aerosol input[61] (Fig. 4e) should favor low altitude summer clouds with more numerous and smaller cloud droplets, which would dampen ice melt by decreasing SW transmittance and increase cloud albedo (Fig. 4e). Smaller droplets will also tend to result in thicker (due to increased water vapor consumption efficiencies) and longer-lived (due to reduced collection efficiencies suppressing rain processes) clouds[62] (note that ice particles in mixed phase clouds also impact cloud lifetimes and liquid water content).

The 'ice melt-cloud optics' positive feedback hypothesized above would predict a continuous decrease in CCN and Nd throughout the summer but, instead, we see a maximum Nd depletion rate in early June that progressively slows through July (Fig. 3b) before becoming slightly positive during August and September (Fig. 3b). These observations suggest a counteracting negative feedback that, according to the hypothesis above, involves a new supply of aerosol. We speculate that a key element in this negative feedback may be primary marine aerosol (sea salt, organic matter) sourcing from the Arctic ocean[63] (Fig. 4c). The rate of sea ice melt in early summer will positively correlate with open ocean area later in the summer and, accordingly, average wind fetch[63-64], growing season length[11], and plankton production[11]. Thus, rapid (slower) early summer CCN removal by precipitation may subsequently trigger enhanced (smaller) ocean aerosol emissions during high (low) sea ice melt summers[64], effectively creating a negative feedback that constrains year-to-year differences in SSIE (Fig. 4c,f). Other processes are almost certainly also at play in this feedback and may include increased terrestrial (e.g., biomass burning) and anthropogenic aerosol emissions during years of rapid sea ice retreat[52,61,64].

Summary

Understanding Arctic sea-ice variability at different time scales is crucial for better predicting future conditions[5] and their ecological[65], climate[66], and economic[67] implications. While natural climate oscillations and anthropogenic greenhouse warming play important roles in longer term SSIE change, these forcings are weakly correlated with the year-to-year variations in SSIE occurring over the CALIOP record (**Methods**). We propose that these shorter-term sea-ice dynamics are instead strongly influenced by feedback mechanisms involving clouds, aerosols, snow/ice albedo, and biology. Previous studies have shown that year-to-year variations in CF are of particular importance during spring[19,43], while we suggest that subsequent changes in cloud optical properties are critical during the core summer ice melt period (Fig. 4). Our 'working hypothesis' proposes that summer cloud optical properties carry with them a 'signature' of the preceding spring CF-driven ice melt while also reflecting summertime variations in aerosol transport and local sourcing, and that it is this time-integration of multiple processes that makes low-altitude summer cloud optical properties such a strong predictor of SSIE (Fig. 2).

Radiative heating of the Arctic surface plays a fundamental role in annual sea-ice cycles. This energy flux is very sensitive to changes in cloud properties (CF, optical depth, cloud type, microphysics) and albedos of underlying melting surfaces[18-19,22]. Satellite lidar measurements are advantageous for Arctic research[24] because they clearly distinguish cloud signals from underlying surface signals and provide accurate measurements of cloud optical properties[25-29]. The discoveries reported here were made possible by these unique lidar capabilities. While we find a remarkable correspondence between year-to-year SSIE variability and summer cloud optical property and radiative budget changes (Fig. 2), Arctic cloud microphysics are complex due to mixtures of liquid and ice particles and the Arctic system as a whole responds to a wide range of forcings (e.g., climate oscillations[5-8], anomalous storms[68]). Motivated by our findings, many opportunities remain for future field and modeling studies to fully resolve this complexity and mechanistic underpinnings of climate forcings in the Arctic system.

References

1. Day, J.J., Hargreaves, J.C., Annan, J.D., Abe-Ouchi, A. Sources of multi-decadal variability in Arctic sea ice extent. *Env. Res. Lett.* 7(3), p.034011 (2012).

2. Docquier, D., Koenigk, T. A review of interactions between ocean heat transport and Arctic sea ice. *Env. Res. Lett.* 16(12), p.123002 (2021).

3. Devasthale, A., Sedlar, J., Koenigk, T., Fetzer, E.J. The thermodynamic state of the Arctic atmosphere observed by AIRS: comparisons during the record minimum sea ice extents of 2007 and 2012. *Atmos. Chem. Phys.* 13, 7441-7450 (2013).

4. Deng, J., Dai, A. Sea ice–air interactions amplify multidecadal variability in the North Atlantic and Arctic region. *Nat. Commun*. 13, 2100 (2022).

5. Karami, M.P., Koenigk, T., Tremblay, B. Variability modes of September Arctic sea ice: drivers and their contributions to sea ice trend and extremes. *Env. Res.: Clim.* 2, p.025005 (2023).

6. Belchansky, G.I., Douglas, D.C., Platonov, N.G. Duration of the Arctic sea ice melt season: Regional and interannual variability, 1979–2001. *J. Clim.* 17, 67-80 (2004).

7. Miles, M.W., Divine, D.V., Furevik, T., Jansen, E., Moros, M., *et. al*. A signal of persistent Atlantic multidecadal variability in Arctic sea ice. *Geophys. Res. Lett.* 41, 463-469 (2014).

8. Cai, Q., Beletsky, D., Wang, J., Lei, R. Interannual and decadal variability of Arctic summer sea ice associated with atmospheric teleconnection patterns during 1850–2017. *J. Clim.* 34, 9931-9955 (2021).

9. Min, S.K., Zhang, X., Zwiers, F.W., Agnew, T. Human influence on Arctic sea ice detectable from early 1990s onwards. *Geophys. Res. Lett.* 35(21) (2008).

10. Intergovernmental Panel on Climate Change. Climate Change 2013: The Physical Science Basis. Working Group I Contribution to the Fifth Assessment Report of the Intergovernmental Panel on Climate Change, edited by T. F. Stocker et al., 1535 pp., Cambridge Univ. Press, Cambridge, U. K., and New York (2013).

11. Arrigo, K.R., van Dijken, G.L. Continued increases in Arctic Ocean primary production. *Prog. Oceanogr*. 136, 60-70 (2015).

12. Arrigo, K.R., van Dijken, G., Pabi, S. Impact of a shrinking Arctic ice cover on marine primary production. *Geophys. Res. Lett.* 35(19) (2008).

13. Derocher, A.E., Lunn, N.J., Stirling, I. Polar bears in a warming climate. *Integr. Compar. Biol.* 44, 163-176 (2004).

14. Moore, S.E., Laidre, K.L. Trends in sea ice cover within habitats used by bowhead whales in the western Arctic. *Ecol. Appl.* 16(3), pp.932-944 (2006).

15. Kovacs, K.M., Lydersen, C., Overland, J.E., Moore, S.E. Impacts of changing sea-ice conditions on Arctic marine mammals. *Mar. Biodiv.* 41, 181-194 (2011).

16. Timmermans, M.L. Marshall, J. Understanding Arctic Ocean circulation: A review of ocean dynamics in a changing climate. *J Geophys. Res.: Oceans* 125(4), p.e2018JC014378 (2020).

17. De Silva, L.W.A., Yamaguchi, H., Ono, J. Ice–ocean coupled computations for sea-ice prediction to support ice navigation in Arctic sea routes. *Polar Res.* 34, p.25008 (2015).

18. Kay, J.E., Gettelman, A. Cloud influence on and response to seasonal Arctic sea ice loss. *J. Geophys. Res.: Atmos.* 114(D18) (2009).

19. Eastman, R., Warren, S.G. Arctic cloud changes from surface and satellite observations. *J. Clim.* 23, 4233-4242 (2010).

20. Kapsch, M.L., Graversen, R.G., Tjernström, M. Springtime atmospheric energy transport and the control of Arctic summer sea-ice extent. *Nat. Clim. Change* 3, 744-748 (2013).

21. Morrison, H., De Boer, G., Feingold, G., Harrington, J., Shupe, M.D., *et. al*. Resilience of persistent Arctic mixed-phase clouds. *Nat. Geosci*. 5, 11–17 (2012).

22. Curry, J.A., Ebert, E.E. Annual cycle of radiation fluxes over the Arctic Ocean: Sensitivity to cloud optical properties. *J. Clim.* 5, 1267-1280 (1992).

23. Winker, D. M., M. A. Vaughan, A. Omar, Y. X. Hu, K. A. Powell, *et. al*. Overview of the CALIPSO Mission and CALIOP data processing algorithms. *J. Atmos. Oceanic Technol*. 26, 2310–2323 (2009).

24. Morrison, A. L., Kay, J. E., Chepfer, H., Guzman, R. Yettella, V. Isolating the liquid cloud response to recent Arctic sea ice variability using spaceborne lidar observations. *J. Geophys. Res.: Atmos*. 123, 473–490 (2018).

25. Hu, Y. Depolarization ratio–effective lidar ratio relation: Theoretical basis for space lidar cloud phase discrimination. *Geophys. Res. Lett.* 34(11) (2007).

26. Hu, Y., Winker, D., Vaughan, M., Lin, B., Omar, A., *et al*. CALIPSO/CALIOP cloud phase discrimination algorithm. *J. Atmos. Ocean. Tech*. 26, 2293-2309 (2009).

27. Oreopoulos, L., Davies, R. Plane parallel albedo biases from satellite observations. Part II: Parameterizations for bias removal. *J. Clim*. 11, 933-944 (1998).

28. Li, Z., H.W. Barker, L. Moreau. The variable effect of clouds on atmospheric absorption of solar radiation. *Nature* 376, 486-490 (1995).

29. Hu, Y., Lu, X., Zhai, P.W., Hostetler, C.A., Hair, J.W., *et. al*. Liquid phase cloud microphysical property estimates from CALIPSO measurements. *Front. Rem. Sens*. 2, 724615 (2021).

30. Behrenfeld, M.J., Hu, Y., Hostetler, C.A., Dall'Olmo, G., Rodier, S.D., *et al*. Space-based lidar measurements of global ocean carbon stocks. *Geophys. Res. Lett*. 40, 4355-4360 (2013).

31. Behrenfeld, M.J., Hu, Y., O'Malley, R.T., Boss, E.S., Hostetler, C.A., *et al*. Annual boom–bust cycles of polar phytoplankton biomass revealed by space-based lidar. *Nature Geosci*. 10, 118-122 (2017).

32. Tan, I., Barahona, D., Coopman, Q. Potential link between ice nucleation and climate model spread in Arctic amplification. *Geophys. Res. Lett*. 49(4), p.e2021GL097373 (2022).

33. Bennartz, R., Shupe, M.D., Turner, D.D., Walden, V.P., Steffen, K, *et al.* July 2012 Greenland melt extent enhanced by low-level liquid clouds. *Nature* 496, 83-86 (2013).

34. Curry, J.A., Rossow, W.B., Randall, D., Schramm, J.L. Overview of Arctic cloud and radiation characteristics. *J. Clim*. 9, 1731-1764 (1996).

35. Intrieri, J.M., Fairall, C.W., Shupe, M.D., Persson, P.O.G., Andreas, E.L., *et al*. An annual cycle of Arctic surface cloud forcing at SHEBA. *J. Geophys. Res.: Oceans* 107(C10) (2002).

36. Shupe, M.D., Intrieri, J.M. Cloud radiative forcing of the Arctic surface: The influence of cloud properties, surface albedo, and solar zenith angle. *J. Clim*. 17, 616-628 (2004).

37. Järvinen, E., Nehlert, F., Xu, G., Waitz, F., Mioche, G., *et al*. Investigating the vertical extent and short-wave radiative effects of the ice phase in Arctic summertime low-level clouds. *Atmos. Chem. Phys*. 23, 7611–7633 (2023).

38. Zhao, M., Wang, Z. Comparison of Arctic clouds between European Center for Medium-Range Weather Forecasts simulations and Atmospheric Radiation Measurement Climate Research Facility long-term observations at the North Slope of Alaska Barrow site. *J. Geophys. Res.: Atmosph.* 115(D23) (2010).

39. Zhang, D., Vogelmann, A., Kollias, P., Luke, E., Yang, F., *et al.* Comparison of Antarctic and Arctic single-layer stratiform mixed-phase cloud properties using ground-based remote sensing measurements. *J. Geophys. Res.: Atmosph.* 124, 10186-10204 (2019).

40. Mioche, G., Jourdan, O., Ceccaldi, M., Delanoë, J. Variability of mixed-phase clouds in the Arctic with a focus on the Svalbard region: a study based on spaceborne active remote sensing. *Atmosph. Chem. Phys*. 15, 2445-2461 (2015).

41. Koren, I., Remer, L.A., Altaratz, O., Martins, J.V., Davidi, A. Aerosol-induced changes of convective cloud anvils produce strong climate warming. *Atmos. Chem. Phys*. 10, 5001-5010 (2010).

42. Huang, Y., Dong, X., Xi, B., Dolinar, E.K., Stanfield, R.E. The footprints of 16 year trends of Arctic springtime cloud and radiation properties on September sea ice retreat. *J. Geophys. Res.: Atmos.* 122, 2179-2193 (2017).

43. Kapsch, M.L., Graversen, R.G., Economou, T., Tjernström, M. The importance of spring atmospheric conditions for predictions of the Arctic summer sea ice extent. *Geophys. Res. Lett.* 41, 5288-5296 (2014).

44. Mason, B.J. The physics of clouds. Oxford Univ. Press. 481 pp (1957).

45. Shaw, G. E. Bio-controlled thermostasis involving the sulfur cycle. *Clim. Change* 5 (5): 297–303 (1983).

46. Field, P.R., Lawson, R.P., Brown, P.R., Lloyd, G., Westbrook, C., *et al.* Secondary ice production: Current state of the science and recommendations for the future. *Meteorol. Monogr.* 58, 7-1 (2017).

47. Burrows, S.M., McCluskey, C.S., Cornwell, G., Steinke, I., Zhang, K., *et al.* Ice-nucleating particles that impact clouds and climate: Observational and modeling research needs. *Rev. Geophys.* 60(2), p.e2021RG000745 (2022).

48. Garrett, T.J., Radke, L.F., Hobbs, P.V. Aerosol effects on cloud emissivity and surface longwave heating in the Arctic. *J. Atmos. Sci.* 59, 769-778 (2002).

49. Reutter P., Su H., Trentmann J., Simmel M., Rose D., *et al*. Aerosol- and updraft-limited regimes of cloud droplet formation: Influence of particle number, size and hygroscopicity on the activation of cloud condensation nuclei (CCN). *Atmos. Chem. Phys*. 9, 7067–7080 (2009).

50. Koren, I., Dagan, G., Altaratz, O. From aerosol-limited to invigoration of warm convective clouds. *Science* 344, 1143-1146 (2014).

51. Twomey, S. Atmospheric aerosols. Elsevier, 287-290 (1977).

52. Willis, M.D., Leaitch, W.R., Abbatt, J.P. Processes controlling the composition and abundance of Arctic aerosol. *Rev. Geophys.* 56, 621-671 (2018).

53. Browse, J., Carslaw, K. S., Arnold, S. R., Pringle, K., Boucher, O. The scavenging processes controlling the seasonal cycle in Arctic sulphate and black carbon aerosol. *Atmos. Chem. Phys*. 12, 6775–6798 (2012).

54. Garrett, T.J., Zhao, C. Increased Arctic cloud longwave emissivity associated with pollution from mid-latitudes. *Nature* 440, 787-789 (2006).

55. Maksimovich, E., Vihma, T. The effect of surface heat fluxes on interannual variability in the spring onset of snow melt in the central Arctic Ocean. *J. Geophys. Res.: Oceans* 117(C7) (2012).

56. Kapsch, M.L., Graversen, R.G., Tjernström, M., Bintanja, R. The effect of downwelling longwave and shortwave radiation on Arctic summer sea ice. *J. Clim.* 29, 1143-1159 (2016).

57. Mortin, J., Svensson, G., Graversen, R.G., Kapsch, M.L., Stroeve, J.C., *et al*. Melt onset over Arctic sea ice controlled by atmospheric moisture transport. *Geophys. Res. Lett.* 43, 6636-6642 (2016).

58. Screen, J.A., Simmonds, I. Declining summer snowfall in the Arctic: Causes, impacts and feedbacks. *Clim. Dynam.* 38, 2243-2256 (2012).

59. Paltridge, G.W. Cloud-radiation feedback to climate. *Quart. J. Roy. Meteor. Soc.* 106, 895-899 (1980).

60. Mauritsen, T., Sedlar, J., Tjernström, M., Leck, C., Martin, M., *et al.* An Arctic CCN-limited cloud-aerosol regime. Atmospheric Chemistry and Physics, 11(1), pp.165-173 (2011).

61. Xian, P., Zhang, J., O'Neill, N.T., Toth, T.D., Sorenson, B., *et al*. Arctic spring and summertime aerosol optical depth baseline from long-term observations and model reanalyses–Part 1: Climatology and trend. *Atmosph. Chem. Phys*. 22, 9915-9947 (2022).

62. Christensen, M.W., Jones, W.K., Stier, P. Aerosols enhance cloud lifetime and brightness along the stratus-to-cumulus transition. Proceedings of the National Academy of Sciences, 117(30), pp.17591-17598 (2020).

63. Leon-Marcos, A., van Pinxteren, M., Zeppenfeld, S., Zeising, M., Bracher, A., *et al*. Thirty Years of Arctic Primary Marine Organic Aerosols: Patterns, Seasonal Dynamics, and Trends (1990–2019). *EGUsphere* 2025, 1-50 (2025).

64. Schmale, J., Sharma, S., Decesari, S., Pernov, J., Massling, A., *et al*. Pan-Arctic seasonal cycles and long-term trends of aerosol properties from ten observatories. *Atmosph. Chem. Phys. Discuss*. 2021, 1-53 (2021).

65. Sumata, H., de Steur, L., Divine, D.V., Granskog, M.A., Gerland, S. Regime shift in Arctic Ocean sea ice thickness. *Nature* 615, 443-449 (2023).

66. Yu, L., Zhong, S. Changes in sea-surface temperature and atmospheric circulation patterns associated with reductions in Arctic sea ice cover in recent decades. *Atmosph. Chem. Phys.* 18, 14149-14159 (2018).

67. Crépin, A.S., Karcher, M., Gascard, J.C. Arctic climate change, economy and society (ACCESS): Integrated perspectives. *Ambio* 46, 341-354 (2017).

68. Parkinson, C.L., Comiso, J.C. On the 2012 record low Arctic sea ice cover: Combined impact of preconditioning and an August storm. *Geophys. Res. Lett.* 40, 1356-1361 (2013).

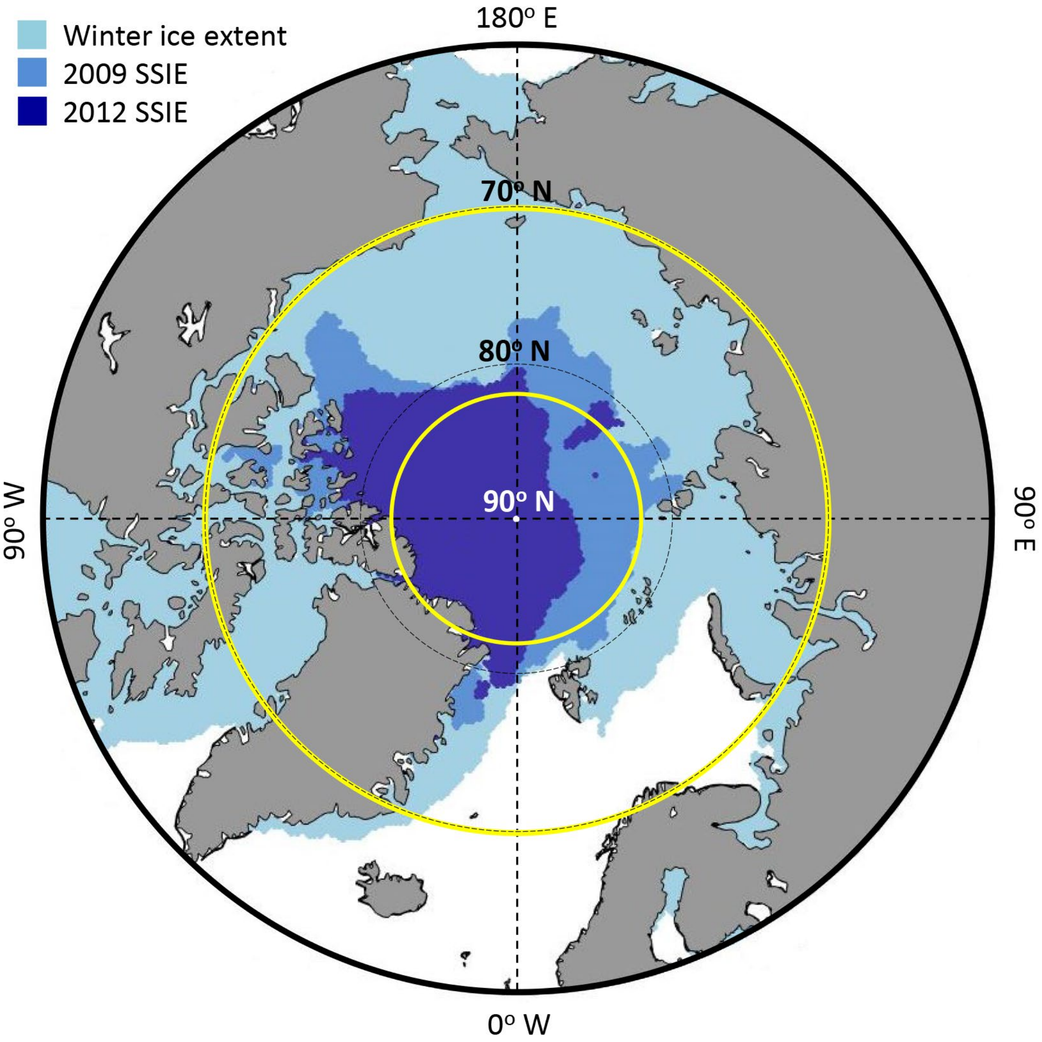

Figure 1. Extremes in Arctic sea-ice extent (SIE) during the CALIOP record. (lightest blue) Average winter sea-ice extent for the CALIOP record. (middle blue) 2009 September sea-ice extent (SSIE). (darkest blue) 2012 SSIE. Yellow lines delineate Arctic region with CALIOP observations (**Methods**).

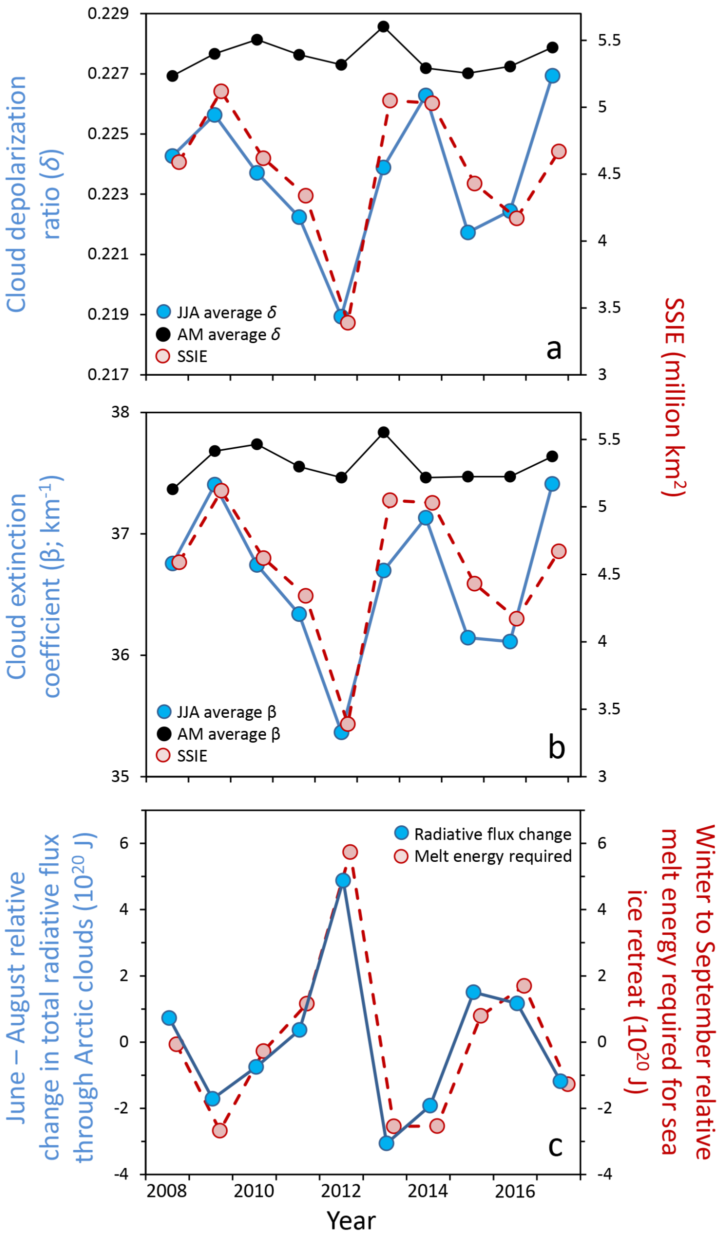

Figure 2. Year-to-year variations in Arctic sea-ice, cloud properties, and melt energy. (a, b) Relationships between September sea-ice extent (SSIE; right axis, red symbols/lines) and April-May (AM) (black symbols/lines) and June through August (JJA) (blue symbols/lines) (a) cloud depolarization and (b) cloud extinction coefficient (left axes). AM values in (a) and (b) are divided by 1.07 and 1.11 to scale with JJA data. (c) Comparison of year-to-year anomalies in total JJA radiative flux through low altitude Arctic clouds (left axis; blue symbols/lines) and melt energy needed to account for observed sea-ice retreat from April to September (right axis, red symbols/lines). Anomalies are calculated as differences relative to the average value for the 2008 to 2017 period. As each data point of the cloud depolarization ratio and extinction coefficient represents averages for millions of cloud profiles, random errors are negligible (i.e., smaller than the size of the symbols in panels).

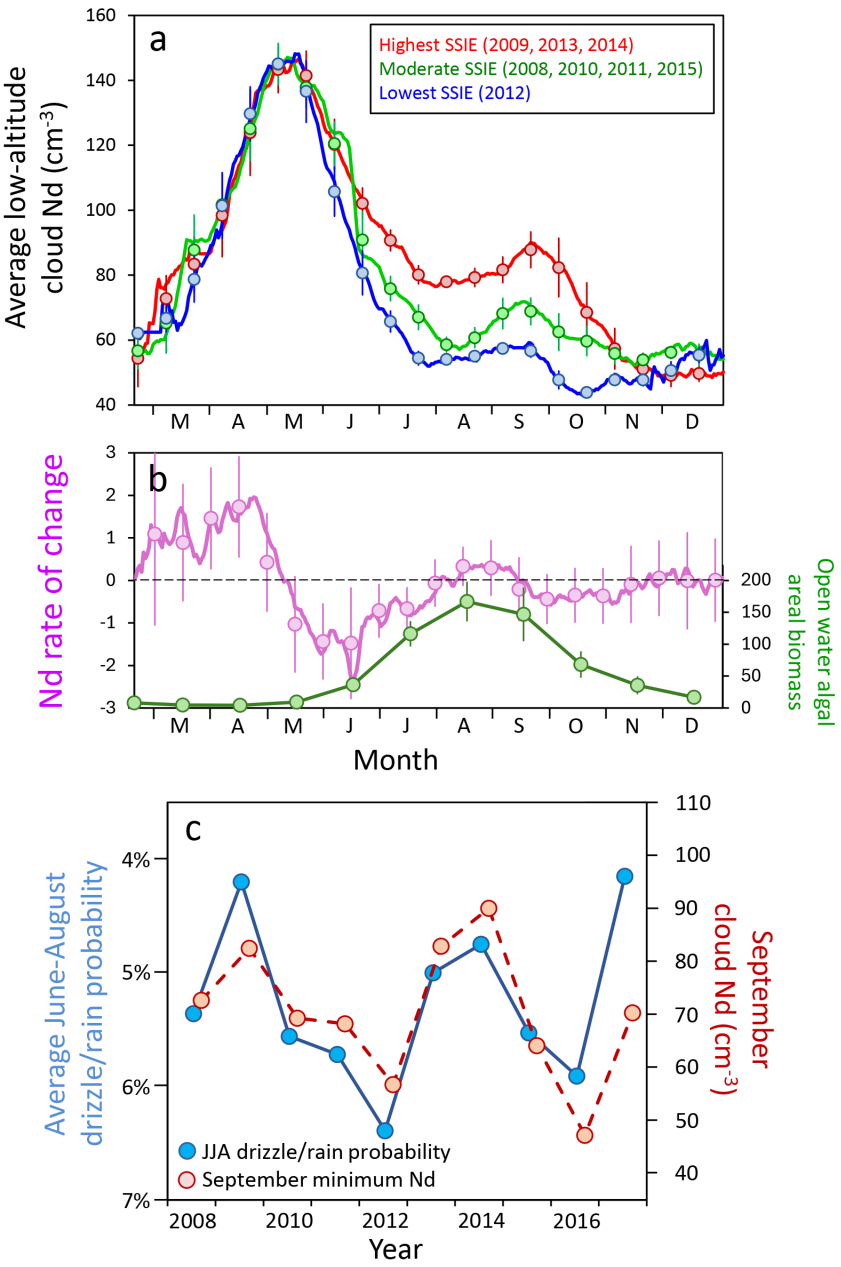

Figure 3. Variability in cloud droplet abundance. (a) Average cloud droplet number concentrations (Nd: cm^{-3}) for (red) highest, (blue) lowest, and (green) moderate September sea-ice extent (SSIE) years. Solid lines = 1 day resolution data. Symbols = 16 day mean values (corresponding to CALIOP's orbit repeat cycle time) with standard deviations indicated by vertical bars. (b) 2008 to 2017 mean rate of change in Nd (cm^{-3} d^{-1}: purple line, left axis) and areal-integrated open-water Arctic monthly mean phytoplankton biomass (Tg C: green line, right axis) (**Methods**). Vertical bars indicate standard deviations for the time series. (c) Relationship between September Nd (right axis, red symbols) and average summer drizzle and rain probability (left axis, blue symbols). As each data point in (c) represents an average for millions of cloud profiles, random errors are negligible (i.e., smaller than the size of the symbols).

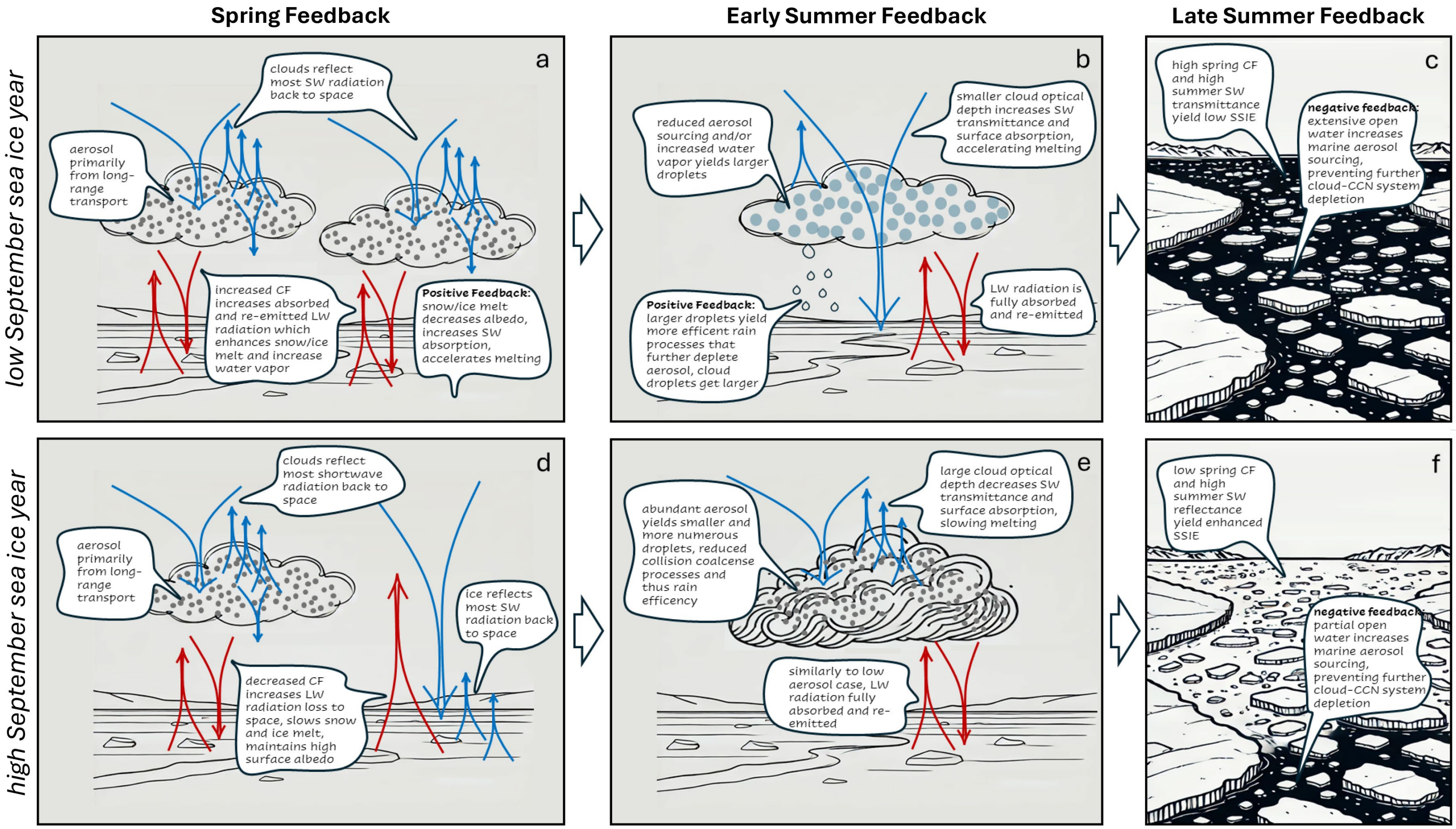

Figure 4. Schematic summary of proposed feedbacks between aerosols, clouds, and September sea-ice extent (SSIE). (a-c) Conditions associated with a low SSIE year. (d-f) Conditions associated with a higher SSIE year. (a,d) As established by previous studies and described in the 'A working hypothesis' section, variations in cloud fraction (CF) play a dominant role in the spring. Compared to low CF years (d), years with high CF (a) exhibit earlier and more extensive ice melt, initially due to longwave (LW) trapping (red arrows) but followed by an increasing contribution from shortwave radiation (SW, blue arrows). Summer processes speculated from our new observations are summarized in panels b, c, e, and f. (b,e) Early summer feedback driven by changes in low-altitude cloud optical properties. (c,f) Late summer feedback involving aerosol sourcing correlated with extent of sea-ice retreat.

These two panels focus on marine aerosol sourcing associated with area of open water, but other terrestrial and/or anthropogenic sources correlated with ice melt may also be important.

Methods

Data Sources

CALIOP data are available at https://asdc.larc.nasa.gov/project/CALIPSO. The CALIPSO spacecraft that carried the CALIOP sensor was launched in 2006 and the mission ended in 2023. The current study evaluates relationships between subtle CALIOP-observed changes in cloud optical properties and Arctic sea-ice retreat. We therefore restricted our analysis to the period with the most reliable and consistent CALIOP data (i.e., 2008 through 2017). Data collected before 2008 were not useable because of an error in the default low/high gain ratio value employed for onboard calculations with the cross-polarized channel[69]. This problem was fixed in late 2007. In 2018, CALIPSO left its A-train orbit to continue flying in formation with the satellite carrying the CloudSat sensor (which had depleted its fuel reserves and could no longer maintain its orbit) (https://www.globe.gov/globe-community/blogs/community-blogs/-/blogs/50544962/maximized). From this point to the end of the CALIPSO mission, CALIOP sampling of the Earth system was no longer consistent with its earlier record and the footprint size of its receiver continued to change with the spacecraft orbit. Because cloud depolarization retrievals are highly sensitive to receiver footprint size, data collected from 2018 onward were considered unreliable for the current analysis.

Sea Ice Extent (SIE) data were obtained from the National Snow and Ice Data Center (https://nsidc.org/data/g02186/versions/1#anchor-data-access-tools). SIE is derived from multi-sensor satellite surface brightness temperature measurements and is taken as the total area in the Arctic with Sea Ice Content (SIC) >15% at each grid box. The uncertainty of SIC over the Arctic is ±5% during winter and increases to ±15% during the summer when melt ponds and wet snow are present on the sea ice[70]. Our SSIE values for > 70°N are offset (lower on average by 0.18 million km^2) than those reported by Huang et al.[71] for > 60°N, but otherwise the two time-series are essentially identical ($r = 0.996$, $p < 0.001$).

Arctic open water algal areal biomass data (Fig. 3b, green line) are calculated from CALIOP-based ocean particulate backscatter coefficients as described in Behrenfeld et al.[31]. As shown in Behrenfeld et al.[31], seasonal cycles in CALIOP-based pan-Arctic phytoplankton biomass values are essentially identical to those based on passive ocean color data from the MODerate-resolution Imaging Spectrometer (MODIS) sensor on the Aqua platform.

For the current study, we defined the Arctic region as poleward of 70°N, however as discussed by Mioche et al.[40] there has been no consensus in the literature on the definition of the Arctic. For example, the Arctic was defined by Mioche et al.[40] as poleward of 60°N, by Kay and Gettleman[18] as poleward of 65°N, by Zygmuntowska et al.[72] as poleward of 68°N for most of the region but poleward of 75°N for the Atlantic section, and by de Boer et al.[73] and Morrison et al.[24] as poleward of 70°N. As illustrated in figure 1 of the current manuscript, delineation at 70°N encompasses the majority of the Arctic ocean while minimizing land area. In Extended Data Fig. 4, we compare our time series of CALIOP-based summer Nd to aerosol optical depth data poleward of 70°N from Xian et al.[61], who referred to this region as the 'high Arctic'. It is noteworthy that Mioche et al.[40] reported that cloud occurrence and mixed-phase cloud occurrence only varied by a few percent for definitions of the Arctic ranging from poleward of 60ºN to poleward of 70ºN.

CALIOP advantages, disadvantages, and uncertainties

As noted in the main manuscript, CALIOP observations provide key advantages for observing Arctic clouds. They allow clear distinction of cloud signals from surface signals, they enable accurate retrieval of cloud optical properties, and they provide nearly a decade of pan-Arctic sampling. In addition, CALIOP has a large receiver footprint diameter (~90 m at the ground)[23] that allows detection of laser light that has been scattered multiple times within clouds. This attribute enables signal retrieval from the surface through the base of most clouds or very deep into thick clouds. The recent study of Hu and Lu[74] analyzing collocated MODIS and CALIOP measurements suggests that CALIOP lidar measurements can detect ground signals through clouds with optical depths of up to 15, which is far greater than the penetration depths achieved by more familiar ground based or airborne lidar systems that have much smaller receiver footprint sizes (thus, limited multiple scattering signal collection). Overall, CALIOP detects the surface signal in ~80% of its Arctic measurements, with the majority of the ~20% remaining cases corresponding to measurements over open water where surface returns are weak.

A disadvantage of CALIOP is that it only conducts measurements along its orbit track at a near nadir angle, whereas passive instruments often collect observations across a broad swath perpendicular to their orbit track. Accordingly, passive sensors such as the MODIS can collect pan-Arctic summer measurements in a single day. In contrast, the orbit repeat cycle of CALIOP only allows pan-Arctic sampling (i.e., not complete spatial coverage) every 16 days. In addition, CALIOP's orbit track does not allow measurements poleward of 82ºN (Fig. 1), which represents 16% of the Arctic area as defined in the current study. To evaluate the general question of whether cloud optical properties measured between 70ºN and 82ºN are representative of the full Artic region poleward of 70ºN, we compared JJA mean cloud optical depths for these two regions using MODIS data (from Level-1 and Atmospheric Archive and Distribution System; https://ladsweb.modaps.eosdis.nasa.gov/archive/allData/62/MCD06COSP_M3_MODIS/). We find that summer cloud properties poleward of 70ºN are well represented ($r = 0.97$, $p < 0.001$) by measured values between 70ºN and 82ºN (Extended Data Figure 5).

Because a satellite lidar only collects vertically-resolved measurement 'curtains' along its orbit track and horizontal averaging is used to reduce random uncertainties, retrieval validation through match-ups with point-source collocated ground measurements is challenging at best. An alternative approach for assessing CALIOP cloud retrieval products is through comparison with co-located passive satellite sensor products over regions where passive products are reliable, noting here that even in these regions passive data still have uncertainties. In Extended Data Figure 3, we show clear relationships between lower latitude MODIS cloud products and CALIOP cloud optical properties. Kay and Gettelman[18] reported a general agreement between cloud properties retrieved by CALIOP, radar, and passive sensors and articulated strengths and weaknesses of each technology. Mioche et al.[40] compared NASA standard CALIOP products, their CALIOP+Radar products, and field measurements and found a general agreement in annual cycles of total cloud occurrence between data sets for the Arctic region as a whole and for the Western Arctic, but discrepancies between data sets in other regions (e.g., Svalbard region).

While direct match-up opportunities are limited between CALIOP cloud products and ground-based Arctic cloud observations, Morrison et al.[24] summarized ground-based, aircraft-based, and satellite-based efforts validating CALIOP cloud detection and classification. Alternative field data sources have been used to evaluate CALIOP retrieved optical properties. In particular, CALIOP's depolarization ratio measurements are used to quantify ocean phytoplankton stocks[29-30]. These ocean observations represent a more challenging retrieval than cloud properties due to the much lower signal strength from the ocean [for ocean retrievals, a 0.1% systematic error results in a 20% bias in the subsurface particulate backscattering coefficient (b_{bp})]. An advantage, however, is that an extensive and sustained global array of autonomous Argo ocean floats is available providing many opportunities for direct match-ups between CALIOP retrievals and field optics measurements. Bisson et al.[75] conducted such an analysis. They used >37,000 float-based ocean b_{bp} observations to create a match-up data set with CALIOP ocean b_{bp} retrievals and reported a median error of $\leq$ 20% and bias of < 10% [74]. Given the difference in signal strength noted above between cloud and ocean signals, these results correspond to a cloud depolarization ratio systematic bias of < 0.1%, implying that the CALIOP depolarization ratio data record can detect small changes in cloud properties.

A fundamental finding of the current investigation is that measured summer mean cloud optical properties are highly correlated with SSIE. For a given lidar pulse, one potential source of uncertainty in retrieved optical properties is the presence of multiple cloud layers and, during the Arctic summer, multilayer clouds are common[34-35]. CALIOP detects these different layers, but some uncertainties still arise because of the weaker signal-to-noise. Nevertheless, retrieval of low-level cloud optical depths is unbiased because it is derived from the depolarization ratio, which is insensitive to attenuation by clouds above. It is noteworthy that layered clouds introduce significant uncertainties in pixel-level retrievals of cloud optical properties using passive satellite sensors[76]. In addition, random uncertainties in cloud optical property retrievals due to cloud layering at the pixel or pulse scale are diminished through spatial averaging. For our pan-Arctic approach, each value for cloud depolarization ratio and extinction coefficient (figure 2a,b) represents the average of millions of cloud profiles, so random errors are near zero. Finally, our analysis is largely based on depolarization ratios and multiple scattering signals from inside clouds and thus are relatively insensitive to solar noise because the cloud signals are much stronger than the sunlight noise.

While the study of Bisson et al.[75] indirectly implies that bias in these CALIOP cloud optical properties is likely very low, this conclusion is difficult to fully verify. If a systematic bias does exist (for example from radiative transfer modeling or lidar calibration) that causes CALIOP products to be under- or over-estimated, it is unlikely to have any significant impact on the correlations we observe with SSIE. Additional uncertainties arise when our CALIOP observed cloud optical properties are used to assess changes in surface radiative budgets for comparison with melt energy requirements for observed sea ice retreat. However, the primary motivation for this additional calculation is to demonstrate that small changes in cloud SW transmittance, when integrated over the cloud-covered Arctic area, can have an impact on surface radiative budgets that is comparable in magnitude to the energy required for the observed sea-ice melt. We note here that the improvement in correlation coefficient for data in figure 2c (r = 0.99) compared to that in figure 2a (r = 0.85) and figure 2b (r = 0.88) results from an accounting for other factors (e.g., cloud fraction, solar zenith angle, surface albedo) influencing surface radiative budgets.

CALIOP retrievals and atmospheric properties

CALIOP depolarization ratio data are calculated from measurements of two polarization channels, are independent of the absolute calibrations of each individual channel, and are retrieved with high accuracy because instrument gain ratios are stable over time. Polarization gain ratio and cross talk data used in this study are monitored and corrected for using both on-board and vicarious sources. The cloud depolarization ratio measurements are also insensitive to changes in atmospheric transmittance above clouds. As a result, CALIOP can detect small changes in cloud depolarization highly accurately. Depolarization by the low-altitude clouds results primarily from multiple scattering by liquid cloud droplets. CALIOP's measured backscatter reflectance is mostly from lower-order scattering. While the vertically resolved lidar return signals measured by CALIOP inherently include signals from ice particles, the contribution of ice particles to pan-Arctic cloud optical properties during the summer period (which is the focus of the current work) is far smaller than that of liquid water droplets. Specifically, the fraction of low-altitude clouds during summer that are mixed phased is generally between 20% and 40% [39-40,77]. Low-altitude summer cloud temperatures are normally above -20 C [77] and have ice water paths that are typically 20% to 40% of total water paths[38,77-80]. Effective liquid droplet diameters are between 10 and 20 µm [29], while summer ice particle diameters are nearly an order of magnitude larger[77,80]. As optical depth can be approximated as ($^3/_2$ × water path) / (effective radius × water density), the contribution of liquid droplets to mixed phase cloud optical depths is more than 20 times that of the far fewer and far larger ice particles. Adding to this the fact that mixed phase clouds generally constitute significantly less than half of total low-altitude clouds, it is clear that the pan-Arctic optical properties of these clouds measured by CALIOP are dominated by liquid water particles.

Details on the CALIOP cloud microphysics derivations (including extinction coefficients, particle sizes, and Nd) are provided in Hu et al.[29] and cloud microphysical data are available at https://drive.google.com/drive/folders/1THUUi4-r46uIke2yqHfedK1zht_4e-NX. Briefly, cloud extinction coefficients are a function of the logarithmic decay of the CALIOP cloud backscatter profile measurements[29], with a multiple scattering correction that depends on cloud depolarization ratios[25]. With the high signal-to-noise ratio of Arctic cloud measurements, there is no systematic error in the logarithmic decay of the CALIOP vertical profile because decay rate is a relative property that does not require absolute calibration. Thus, the systematic biases of the CALIOP cloud extinction coefficients and depolarization ratios are comparable. The cloud extinction coefficient is closely related to the cloud droplet number concentration (Nd), although there is a somewhat larger uncertainty in Nd due to its dependence on absolute channel calibrations[29]. In figures 3a, Nd values are the logarithmic average of droplet density for all the low-altitude clouds. The ratio of CALIOP cross-polarized to co-polarized signals at 532 nm provides a direct and accurate measurement of cloud depolarization[26]. Summer depolarization ratios are linearly proportional to the logarithmically averaged cloud optical depth (Hu & Lu 2024) (Extended Data Fig. 3a), which itself is linearly proportional to cloud reflectance[27] (Extended Data Fig. 3b) and transmittance, as cloud absorptance is near constant at the low solar zenith angles characteristic of the Arctic[28]. Thus, summer cloud transmittance is linearly proportional to measured cloud depolarization.

While depolarization ratios are sensitive to changes of cloud reflectance and transmittance, extinction coefficients are most sensitive to changes of cloud droplet number density (Extended Data Fig. 3c). Results shown in figure 2b suggest that the inter-annual changes of cloud transmittance are most likely due to changes in cloud microphysical properties, such as cloud droplet number density.

Estimation of year-to-year changes in summer radiative budgets and ice melt energy

Measured summer interannual variations in low-altitude cloud optical properties are quantitatively related to changes in summer surface radiative flux in the Arctic. As noted above, the primary motivation for calculating interannual anomalies in summer net radiative heating was to show that small changes in cloud optical properties measured by CALIOP (Fig. 2a,b), when integrated over the cloud-covered Arctic area, can have an impact comparable in magnitude to the melt energy required for observed SSIE variations (Fig. 2c). Each step below allows for a rough estimate that does not take into account all the detailed factors influencing summer radiative heating, but the apparent success of these calculations (Figure 2c) should motivate more rigorous studies in the future. First, we estimated summer net radiative heating (H) of the Arctic surface (open water and sea-ice) as:

$$H \approx A_{sea} \Delta t \left\{ \left[CF\, F_{SW+LW,cloudy,surf} \right] + \left[(1 - CF) F_{SW+LW,clear,surf} \right] \right\} \qquad (1)$$

where:

1. H = summer net radiative heating for a given year,
2. A_{sea} = total area of the Arctic poleward of 70^{o}N,
3. Δt = total time (seconds) between June 1 and September 15 = 9.2448×10^{6} s,
4. $F_{SW+LW,cloudy,surf}$ = net (difference between downward and upward fluxes, accounting for variations in surface albedo and solar zenith angle) downward shortwave (SW) and longwave (LW) radiative fluxes at the surface for a cloudy sky,
5. CF = average Arctic summer low-altitude cloud fraction based on CALIOP measurements (Extended Data Fig. 2), and
6. $F_{SW+LW,clear,surf}$ = June through August (JJA) average net downward SW and LW radiative fluxes at the surface for clear skies.

Year-to-year anomalies in summer net radiative heating (Fig. 2c) were calculated as the difference between H for a given year and the average value of H for the CALIOP 2008-2017 period.

Logarithmically averaged optical depths of low-altitude clouds for the Arctic varied between 6.1 and 6.6 from year to year (Extended Data Fig. 1) and average effective radius derived from CALIPSO varied from 9.3 to 10.1 µm [29]. Thus, average liquid water paths (i.e., $W = \frac{2}{3} \times$ optical depth × radius) varied between 40.07 and 40.92 g m^{-2}, giving a range in summer average downward LW emissivity of clouds (i.e., $1 - e^{-0.158 \times W}$ [81]) of 0.9985 to 0.9987. Year-to-year variations in summer downward LW surface flux are approximated as the downward LW flux of the atmospheric window (~100 W m^{-2}) times 0.0002 = 0.02 W m^{-2}. Since droplet size decreases when optical depth increases, we expect even smaller interannual variations in W and downward LW fluxes. By comparison, interannual variations in transmittance of SW radiation are >10 W m^{-2} due to variations of cloud transmittance of sunlight [i.e., the product of Arctic summer solar insulation and variation in SW transmittance (Extended Data Fig. 1): ~ 480 W m^{-2} × 0.02)] and its surface albedo feedback. Thus, we can assume that year-to-year variations in summer LW forcing is negligible, allowing equation 1 to be simplified to:

$$H \approx A_{sea} \Delta t \left\{ \left[CF\ F_{SWcloudy,surf} \right] + \left[(1 - CF) F_{SW,clear,surf} \right] \right\} \tag{2}$$

Year-to-year variations in net downward SW radiative flux ($F_{SW,cloudy,surf}$) were calculated as a function of low-altitude effective cloud transmissivity ($T_{r,cloud}$), which is a function of cloud optical depth and surface albedo:

$$F_{SW,cloudy,surf} = F_{down,TOA} * T_{r,clear} * (1 - \alpha) T_{r,cloud}(\tau_{cloud}, \alpha), \tag{3}$$

where $F_{down,TOA}$ is average JJA solar insolation = 480 W m^2 [82] and $T_{r,clear}$is average transmissivity of sunlight in the absence of clouds = 80% [83]. Low-altitude water cloud τ values were estimated from CALIOP-measured depolarization ratios using a relationship developed with collocated MODIS optical depths and shown in Extended Data Fig. 3. Associated changes in water cloud transmittance ($T_{r,cloud}$) were then quantified following Fitzpatrick et al.[84] as:

$$T_{r,cloud} = \frac{a + b * \cos\theta}{1 + (c - d\alpha)\tau} = \frac{a_1 + (1 - a_1) e^{-k_1 \tau} + b_1 \left[1 + b_2 e^{-k_2 \tau} + b_3 e^{-k_3 \tau} \right] \cos\theta}{1 + (c - d\alpha)\tau} \tag{4}$$

where a, b, a_1, k_1, b_1, b_2, k_2, k_3, c, d are constants and θ is the solar zenith angle. To assess changes in surface radiative heating due to variations in $T_{r,cloud}$, we assumed an average broadband SW snow/sea-ice surface albedo of ~0.8 and an open ocean surface albedo of ~0.05, giving an average surface albedo (α) of: $\alpha = 0.8 * f_{ice} + 0.05 * (1 - f_{ice})$, where f_{ice} is the average fraction of the Arctic area poleward of 70°N that is ice covered during a given summer. It is important to note here that this dependence on ice cover creates a feedback with cloud optical properties. Specifically, in years with high summer cloud SW transmittance, reflectance from the surface will also be diminished, thus amplifying the summer cloud effect. Quantitatively, summer sea ice cover is correlated with September sea ice cover ($R^2 = 0.63$), but when the radiative impact of these sea ice changes is combined with the impact of changes in summer cloud properties a much greater fraction of SSIE variability is accounted for ($R^2 = 0.93$).

Cloud radiative forcing at the Arctic surface is sensitive to variations in cloud optical depth (τ) and surface albedo. Detecting clouds and estimating τ during the Arctic's core summer melting period has been a major challenge in the past due to the limitations of traditional sensors described above. Thus, large uncertainties have remained in assessments of Arctic cloud radiative forcing at the surface. A critical advantage of CALIOP is that it can clearly distinguish cloud signals from surface signals and it provides consistent estimates of τ and $T_{r,cloud}$ from measured liquid cloud depolarization ratios.

In figure 2c, we show a strong correlation between year-to-year changes in summer surface radiative budgets and the energy needed to account for observed variations in SSIE. This latter energy requirement was estimated using (1) observed changes in sea ice between the end of March and the sea-ice minimum in September, (2) an energy requirement of 334 J to melt a gram of ice, (3) an ice density of $0.917*10^6$ g/m^3, and (4) assuming an end of March Arctic sea-ice mean thickness of 1.5 m for the CALIOP observational record[85].

Drizzle and rain probabilities

In warm clouds, the collision–coalescence process that produces drizzle and rain becomes efficient once characteristic droplet or effective radii grow to O(10–15 µm). A critical droplet size marking the onset of efficient rain formation has been identified in microphysical simulations and observations[90]. Numerous in situ and satellite studies further show that rain initiation is typically associated with cloud-top effective radii of about 12 to 15 µm [90-94]. Guided by this body of work and the recent direct comparison of Cloudsat and CALIPSO precipitation identification[95], we adopted a cloud-top effective radius of 15 µm, together with cloud extinction-to-backscatter ratios (S) < 18, as an empirical threshold for the onset of efficient precipitation processes. The condition $S < 18$ acts as an independent microphysical indicator that the column contains drizzle/rain, complementing the effective-radius threshold[95-96]. Interannual variations in drizzle probability show similar patterns to those shown in figure 3c when we choose other cloud effective radii as the threshold (Extended Data Fig. 6).

Climate Oscillation Indices, Passive Sensor Cloud Properties, and SSIE

Findings reported in the main manuscript evidence strong correlations between SSIE and summertime cloud optical properties. We also investigated whether year-to-year variations in SSIE over the CALIOP record exhibited significant relationships with climate oscillations that have earlier been shown to correlate with longer term SSIE changes[5-8]. Results of this analysis are shown in Table 1 and reveal no statistically significant relationships with these climate oscillation indices.

Table 1. Linear regression statistics for relationships between SSIE and various climate oscillation indices for the CALIOP observational period (2008 – 2017).

Climate Oscillation Index	R^2	p value	Climate Index Data Source
Arctic Multidecadal Oscillation	0.113	> 0.1	https://psl.noaa.gov/data/climateindices/list/
Multivariate ENSO Index	0.001	> 0.1	https://psl.noaa.gov/data/climateindices/list/
North Atlantic Oscillation	0.006	> 0.1	https://psl.noaa.gov/data/climateindices/list/
Pacific Decadal Oscillation	0.028	> 0.1	https://psl.noaa.gov/data/climateindices/list/
Arctic Oscillation	0.007	> 0.1	https://psl.noaa.gov/data/climateindices/list/

We also evaluated whether year-to-year variations in SSIE over the CALIOP record exhibited significant relationships with passive sensor retrievals of summer cloud fraction or liquid water path from CERES and MODIS. Results of this analysis are shown in Table 2 and reveal little to no relationships with SSIE. For this analysis, we used CERES data taken from the synoptic 1 degree (SYN1deg) product[97] downloaded from https://ceres.larc.nasa.gov/ and MODIS data taken from the level-3 globally gridded monthly mean product (MOD08_M3 and MYD08_M3) [98] downloaded from the NASA Level-1 and Atmosphere Archive and Distribution System Distributed Active Archive (https://ladsweb.modaps.eosdis.nasa.gov).

Table 2. R^2 for relationships between SSIE and (second column) CERES and (third column) MODIS passive measurements of cloud fraction and liquid water path in summer (June, July, August) for the CALIOP observational period (2008 – 2017).

Summer Cloud Property	CERES	MODIS
Low cloud fraction	0.27	-
Total cloud fraction	0.005	0.01
Low cloud liquid water path	0.008	-
Total liquid water path	0.005	0.03

Statistical analyses

Linear regression statistics reported in this study are based on Pearson's R. We tested linearity in the relationships between all reported variables for each case by fitting a model and assessing the p values. As noted above, uncertainty associated with CALIOP pan-Arctic data is extremely low. To confirm the high r-values reported herein, we ran a bootstrapping procedure allowing estimation of r-value distributions, which confirmed that all reported relationships are significant.

Data availability

Links to sources of all standard publicly available data used in this study and CALIOP cloud microphysical data are provided in the **Methods** text above and in Table 1. Additional CALIPSO/CALIOP data are available at: https://www.earthdata.nasa.gov/data/tools/asdc-calipso-search-subset-tool. Sea ice extent data downloaded from the National Snow and Ice Data Center were analyzed in Microsoft Excel and are available upon request from lead author M.J.B.

Code availability

Computational code used for the analysis of CALIOP data is available at: https://github.com/tkwestberry/arcticIceNclouds and https://oregonstate.box.com/s/x5g3gsh134tbtonaa44sl786daxcycvc.

Methods section references

69. Behrenfeld, M.J., Gaube, P., Della Penna, A., O'Malley, R.T., Burt, W.J., *et al*. Global satellite-observed daily vertical migrations of ocean animals. *Nature* 576, 257-261 (2019).

70. Cavalieri, D. J., Crawford, J.P., Drinkwater, M.R., Emery, W.J., Eppler, D.T., *et al*. NASA Sea Ice Validation Program for the DMSP SSM/I: Final Report, NASA Technical Memorandum 104559, National Aeronautics and Space Administration, https://ntrs.nasa.gov/api/citations/19920015007/downloads/19920015007.pdf (1992).

71. Huang, Y., Ding, Q., Dong, X., Xi, B., Baxter, I. Summertime low clouds mediate the impact of the large-scale circulation on Arctic sea ice. *Comm. Earth Envir.* 2(1), p.38 https://doi.org/10.1038/s43247-021-00114-w (2021).

72. Zygmuntowska, M., Mauritsen, T., Quaas, J., Kaleschke, L. Arctic Clouds and Surface Radiation–a critical comparison of satellite retrievals and the ERA-Interim reanalysis. *Atmosph. Chem. Phys.* 12, 6667-6677 (2012).

73. de Boer, G., Chapman, W., Kay, J.E., Medeiros, B., Shupe, M.D., *et al*. A characterization of the present-day Arctic atmosphere in CCSM4. *J. Clim.* 25, 2676-2695 (2012).

74. Hu, K., Lu, X. Spaceborne lidar measurement of global cloud properties through machine learning. *Front. Remote Sens*. 5, p.1477503 (2024).

75. Bisson, K.M., Boss, E., Werdell, P.J., Ibrahim, A., Behrenfeld, M.J. Particulate backscattering in the global ocean: a comparison of independent assessments. *Geophys. Res. Lett*. 48, p.e2020GL090909 (2021).

76. Marchant, B., Platnick, S., Meyer, K., Wind, G. Evaluation of the MODIS Collection 6 multilayer cloud detection algorithm through comparisons with CloudSat Cloud Profiling Radar and CALIPSO CALIOP products. *Atmos. Meas. Tech.* 13, 3263–3275 (2020).

77. Shupe, M.D., Matrosov, S.Y., Uttal, T. Arctic mixed-phase cloud properties derived from surface-based sensors at SHEBA. *J. Atmosph. Sci*. 63, 697-711 (2006).

78. Yang, J., Zhang, Y., Wang, Z., Zhang, D. Cloud Type and Life Stage Dependency of Liquid–Ice Mass Partitioning in Mixed-Phase Clouds. *Remote Sens*. 14, 1431. (2022).

79. Achtert, P., O'Connor, E. J., Brooks, I. M., Sotiropoulou, G., Shupe, M. D., *et al*. Properties of Arctic liquid and mixed-phase clouds from shipborne Cloudnet observations during ACSE 2014. *Atmos. Chem. Phys.* 20, 14983–15002, (2020).

80. Ong, C. R., Koike, M., Hashino, T., Miura, H. Responses of simulated Arctic mixed-phase clouds to parameterized ice particle shape. *J. Atmos. Sci.* 81, 125-152 (2024).

81. Stephens, G.L., Paltridge, G.W., Platt, C.M.R. Radiation profiles in extended water clouds. III: Observations. *J. Atmos. Sci.* 35, 2133-2141 (1978).

82. Prince, H.D., L'Ecuyer, T.S. Observed energetic adjustment of the Arctic and Antarctic in a warming world. *J. Clim*. 37, 2611-2627 (2024).

83. Wild, M., Hakuba, M.Z., Folini, D., Dörig-Ott, P., Schär, C., *et al*. The cloud-free global energy balance and inferred cloud radiative effects: an assessment based on direct observations and climate models. *Clim. Dyn.* 52, 4787–4812 (2019).

84. Fitzpatrick, M.F., Brandt, R.E., Warren, S.G. Transmission of solar radiation by clouds over snow and ice surfaces: A parameterization in terms of optical depth, solar zenith angle, and surface albedo. *J. Clim*. 17, 266-275 (2004).

85. Cuevas, C.A., Maffezzoli, N., Corella, J.P., Spolaor, A., Vallelonga, P., *et al*. Rapid increase in atmospheric iodine levels in the North Atlantic since the mid-20th century. *Nature Comm.* 9, 1452 (2018).

86. Nakajima, T., K. Suzuki, G.L. Stephens. Droplet growth in warm water clouds observed by the A-Train. Part I: Sensitivity analysis of the MODIS-derived cloud droplet sizes. *J. Atmos. Sci*. 67, 1884-1896 (2010).

87. Stephens, G.L., Pelon, J., Winker, D., Trepte, C.,Vane, D. CloudSat and CALIPSO within the A-Train: Ten years of actively observing the Earth system. *Bull Amer. Met Soc.* doi:10.1175/BAMS-D-16-0324.1 (2018).

88. Takahashi, H., K. Suzuki, G.L. Stephens. Land–ocean differences in the warm-rain formation process in satellite and ground-based observations and model simulations; Q. J. R. *Meteorol. Soc*. doi:10.1002/qj.3042 (2017).

89. Platnick, S., Meyer, K.G., King, M.D., Wind, G., Amarasinghe, N., *et al.*The MODIS cloud optical and microphysical products: Collection 6 updates and examples from Terra and Aqua. *IEEE Trans.Geosci. Rem. Sens*. 55, 502-525 (2016).

90. Khain, A., Prabha, T.V., Benmoshe, N., Pandithurai, G., Ovchinnikov, M. The mechanism of first raindrops formation in deep convective clouds. *J. Geophys. Res.: Atmos*. 118, 9123-9140 (2013).

91. Rosenfeld, D., Gutman, G. Retrieving microphysical properties near the tops of potential rain clouds by multispectral analysis of AVHRR data. *Atmos. Res*. 34, 259-283 (1994).

92. Rosenfeld, D., Wang, H., Rasch, P.J. The roles of cloud drop effective radius and LWP in determining rain properties in marine stratocumulus. *Geophys. Res. Lett*. 39(13) (2012).

93. Kulkarni, J.R., Maheskumar, R.S., Morwal, S.B., Kumari, B.P., Konwar, M., *et al*. The cloud aerosol interaction and precipitation enhancement experiment (CAIPEEX): overview and preliminary results. *Curr. Sci*. pp. 413-425 (2012).

94. Braga, R. C., Rosenfeld, D., Krüger, O. O., Ervens, B., Holanda, B. A., *et al*. Linear relationship between effective radius and precipitation water content near the top of convective clouds: measurement results from ACRIDICON–CHUVA campaign. *Atmos. Chem. Phys*. 21, 14079–14088 (2021).

95. Zeng, S., Hu, Y., Vaughan, M., Trepte, C., Liu, Z., Omar, A., *et al*. Identification of precipitating marine low-altitude water clouds by CALIPSO: Observations and detections. *J. Geophys. Res.: Atmos*. 130, p.e2025JD043401 (2025).

96. Gayet, J.F., Stachlewska, I.S., Jourdan, O., Shcherbakov, V., Schwarzenboeck, A. *et al*. Microphysical and optical properties of precipitating drizzle and ice particles obtained from alternated lidar and in situ measurements. In: *Annales Geophysicae* (Vol. 25, No. 7, pp. 1487-1497). Göttingen, Germany: Copernicus Publications (2007)

97. Doelling, D.R., Loeb, N.G., Keyes, D.F., Nordeen, M.L., Morstad, D., *et al.* Geostationary Enhanced Temporal Interpolation for CERES Flux Products. *J. Atmos. Ocean. Techn*. 30, 1072-1090 (2013).

98. King, M.D., Platnick, S., Menzel, W.P., Ackerman, S.A., Hubanks, P.A. Spatial and temporal distribution of clouds observed by MODIS onboard the Terra and Aqua satellites. *IEEE Trans. Geosci. Rem. Sens.* 51, 3826–3852 (2013).

Acknowledgments: The authors thank Professor Kimberly Halsey for constructive feedback on the manuscript, Toby Westberry for assistance with analyzing MODIS cloud optical depth data, and Peng Xian and two anonymous reviewers for thoughtful and constructive comments during the formal review that resulted in a significantly improved manuscript and new insight on the potential role of year-to-year variations in aerosol transport from lower latitudes.

Funding:

National Aeronautics and Space Administration grants 80NSSC24K0446, 80NSSC22K0358, and 80NSSC21K0414 (MJB), NASA Interdisciplinary Studies funding (YH).

Author contributions:

Conceptualization: MJB, YH
Methodology: YH, MJB
Investigation: MJB, YH
Visualization: MJB, YH, KB, IK
Writing – original draft: MJB
Writing – review & editing: All authors

Competing interests:

Authors declare that they have no competing interests.

Supplementary information: Extended data figures 1 to 6.

Corresponding authors: Michael J. Behrenfeld (Michael.Behrenfeld@oregonstate.edu) and Yongxiang Hu (yxhuva@gmail.com)

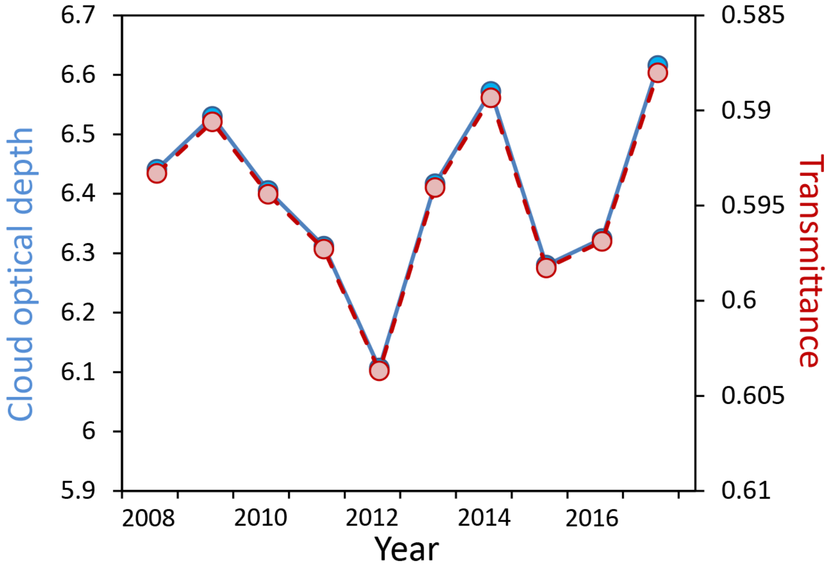

Extended Data Fig. 1: Year-to-year variations in mean summer (June through August) cloud optical depth (τ; unitless) and transmittance (unitless). Values of τ (left axis) are calculated using CALIOP measured cloud depolarization ratios (Extended Data Fig. 3a) and reflectance (Extended Data Fig. 3b) following methods described in Hu and Lu[73]. Transmittance is calculated using cloud optical depth, solar zenith, and surface albedo following methods described in Hu et al.[28]. As each data point represents an average for millions of cloud profiles, random errors are negligible (i.e., smaller than the size of the symbols).

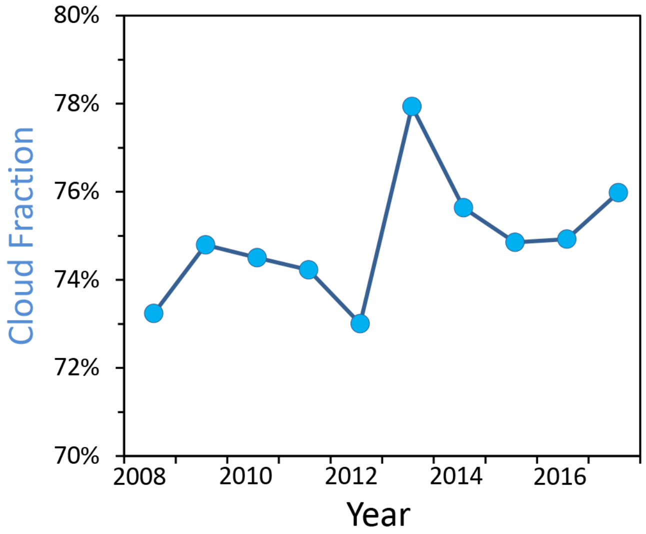

Extended Data Fig. 2: Mean June through August (JJA) Arctic cloud fraction (CF) for each year of the CALIOP record**.** Note the small absolute range of the y-axis.

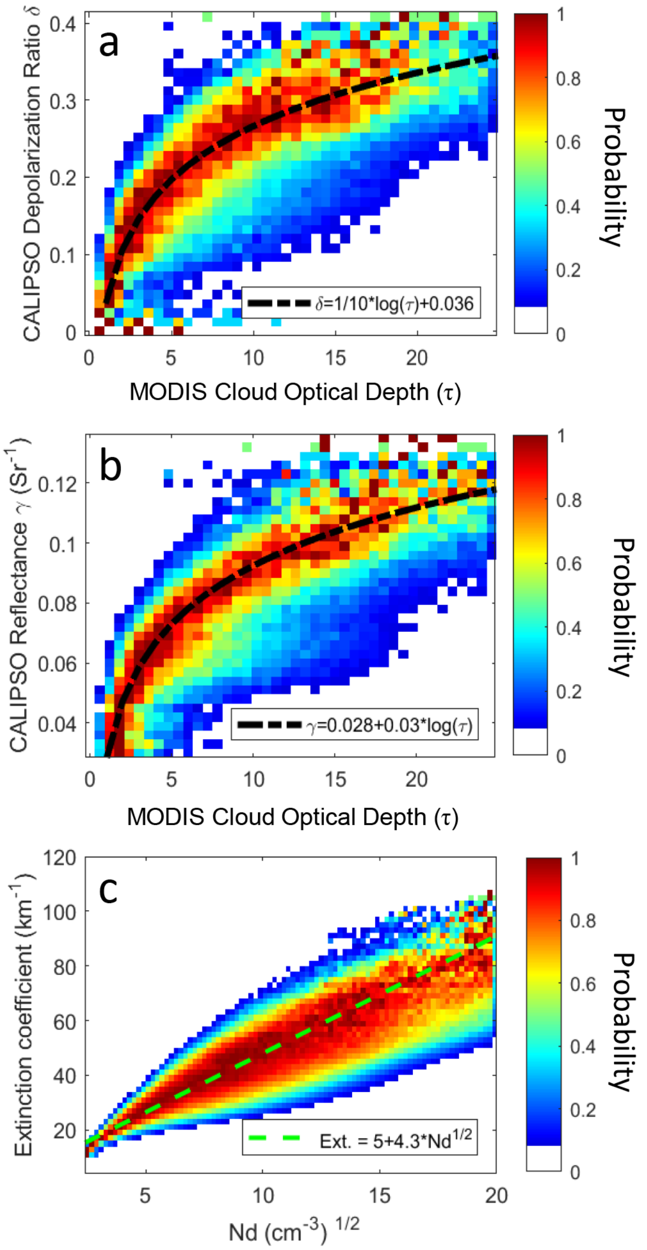

Extended Data Fig. 3: Relationships between key cloud properties. (a) CALIOP measured cloud depolarization ratios (δ) and coincident cloud optical depths (τ) retrieved with the Moderate Resolution Imaging Spectrometer (MODIS). (b) CALIOP measured cloud reflectance (γ) and MODIS τ. (c) CALIOP measured cloud extinction coefficient and cloud droplet number concentration (Nd). The heatmap color bars in panels a and b represent the relative probability of the CALIOP cloud depolarization ratio and reflectance for a specific cloud optical depth measured by MODIS, respectively. The heatmap color bar in panel c is the probability of an extinction coefficient for a given cloud droplet number density (Nd) from CALIOP. Relationships shown in this figure between CALIOP and MODIS observations are based on measurements for stratiform clouds over a dark ocean at lower latitudes where multi-layer cloud scenes have been filtered out. Under these conditions, MODIS optical depth data are considered validated products. The relationship between CALIOP cloud depolarization ratio and MODIS cloud optical depth (panel a) is applied to CALIOP cloud depolarization data for the Arctic where MODIS cloud optical depth data are not reliable.

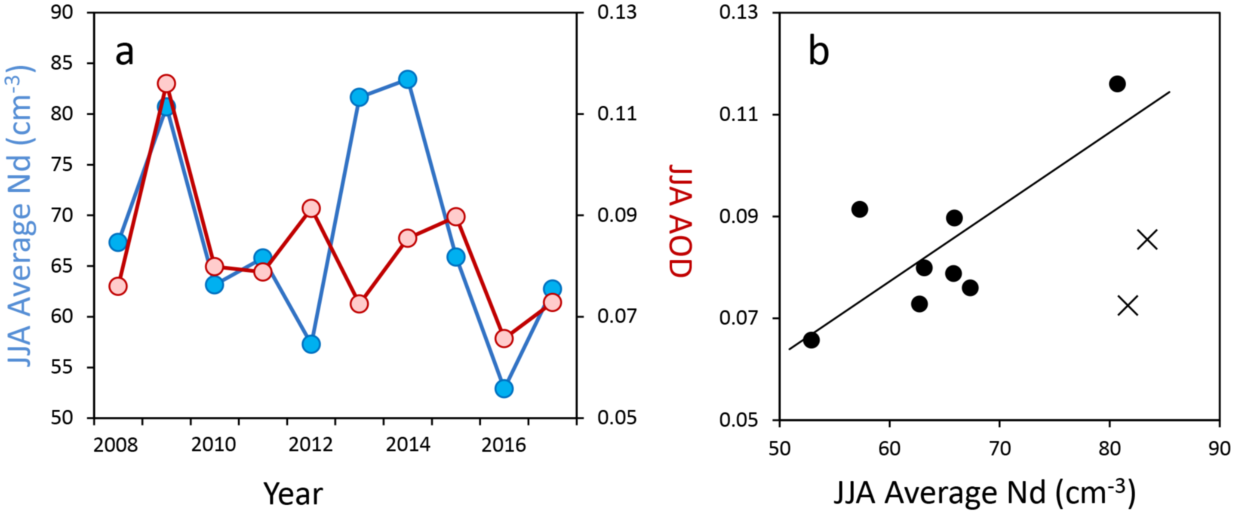

Extended Data Figure 4. Relationship between Arctic summer (June-August) average cloud droplet abundance (Nd) and aerosol optical depth (AOD). (a) Time series of CALIOP Nd and AOD from Xian et al.[60]. (b) Scatterplot of Nd versus AOD. Solid symbols = data from panel a excluding data for 2013 and 2014 . X symbols = 2013 and 2014 data. Linear regression analysis based on all years gives an r value of 0.17 and p value of 0.23. Linear regression analysis for all years excluding 2013 and 2014 gives an r value of 0.77 and p value of 0.02. Year to year variability in JJA AOD is significantly influenced by transport from terrestrial sources[60]. Results presented in panels a and b suggest that variability in summer aerosol transport to the Arctic may in part contribute to variability in low altitude cloud optical properties, at least for some years (e.g., other factors may have been particularly influencial during 2013 and 2014). AOD values are the mean of three reanalysis products described in Xian et al.[60] for latitudes >70ºN. Note that AOD is a column integrated atmospheric property whereas CALIOP Nd data are for low-altitude clouds.

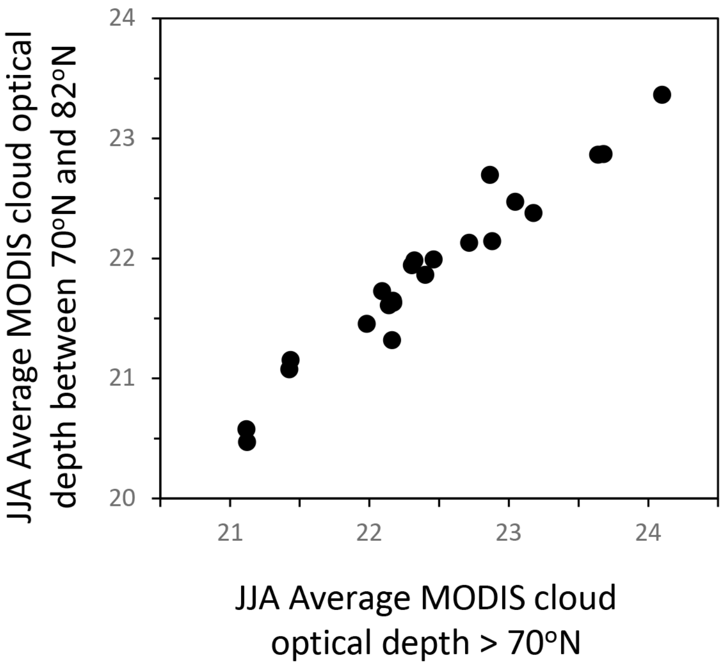

Extended Data Figure 5. Relationship between Arctic summer (June-August) average cloud optical depth for observations poleward of 70ºN and observations between 70ºN and 82ºN. Data are based on MODIS observations between 2003 and 2024 (**Methods**) and the cloud optical depth algorithm of Platnick et al.[88]. The 70ºN to 82ºN zone corresponds to the Arctic region where CALIOP observations are available.

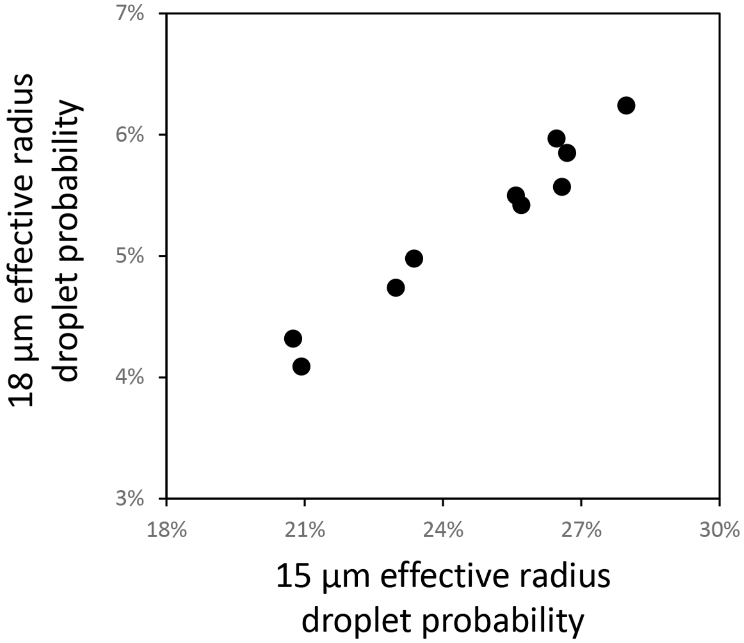

Extended Data Figure 6. Relationship between probabilities of 15 µm versus 18 µm effective radius low-altitude cloud droplets for the Arctic summer (June-August). Data represent year-specific pan-Arctic summer average values over the 2008 to 2017 CALIOP record. In figure 3c of the main manuscript, we show a significant correlation between September cloud droplet number concentrations (Nd) and average summer drizzle/rain probabilities based on droplet effective radii of 15 µm. Very similar relationships are found with Nd if we chose other cloud effective radii as the threshold, as indicated in the above panel by the strong correlation ($r = 0.98$, $p < 0.001$) between probabilities of effective droplet radii of 15 µm and 18 µm.